Crowding-Induced Anisotropic Transport Modulates Reaction Kinetics in Nanoscale Porous Media

R. Grima,[†,‡,¶] S. N. Yaliraki,[†,§,#] and M. Barahona*[,†,∥]

Institute for Mathematical Sciences, Department of Chemistry, and Department of Bioengineering, Imperial College London, United Kingdom

Received: March 22, 2009; Revised Manuscript Received: March 1, 2010

We quantify the emergence of persistent anisotropy in the diffusion of spherical tracer particles through a nanoscale porous medium composed of a uniform distribution of purely symmetric crowding particles. We focus on the interior of a biological cell as an example of such a medium and find that diffusion is highly directional for distances comparable to the size of some organelles. We use a geometrical procedure that avoids the standard orientational averaging to quantify the anisotropy of diffusive paths and show that the point source distributions are predominantly of prolate ellipsoidal shape as a result of local volume exclusion. This geometrical symmetry breaking strongly skews the distribution of kinetic rates of diffusion-limited reactions toward small values, leading to the result that, for short to intermediate times, almost 80% of the rates measured in an ensemble of heterogeneous media are smaller than the expected rate in an ideal homogeneous medium of similar excluded volume fraction. This crowding-induced modulation may have implications for our understanding and measurement of diffusion-controlled intracellular reaction kinetics and for experimental nanotechnology applications, such as nanoparticle-based bioimaging and drug delivery, where diffusion plays an important role.

Introduction

Porous media with structural features at the nanoscale are ubiquitous in nature.[1] The characterization of such media is key for our understanding of transport and reaction kinetics in crowded cellular environments[2–4] and, consequently, for improved applications in the area of bionanotechnology,[5] including nanoparticle-based platforms for extra- and intracellular drug delivery,[6–8] bioimaging,[9,10] and biosensing.[11] A large body of research has been devoted to characterizing the deviations from ideal diffusion of transport in porous media by elucidating the dependence of *average macroscopic* transport[1] on structural properties of the medium. In this traditional approach, the effects of local inhomogeneities of the medium are *averaged out* when describing transport at the macroscopic level. However, recent experimental advances in single-particle tracking have brought to the fore the importance of the local topological features for transport in such crowded environments.[4,12]

Here, we quantify through numerical simulation and analysis the diffusion anisotropy imposed by the locally heterogeneous crowding environment and we illustrate how this phenomenon has a strong bearing on reaction kinetics. We first show that the inhomogeneities in the medium translate into anisotropic transport that becomes long-lived in crowded environments, even if the medium is mesoscopically isotropic, i.e., constituted by a uniform distribution of spherical particles. We characterize this anisotropy with a gyration tensor, which could be obtained from experimental data, and show that the spatial distribution of diffusive particles in crowded environments will be dominantly prolate (egg-like), corresponding to diffusive exploration along quasi-one-dimensional local paths.

This crowding-induced anisotropic diffusion has a major effect on reaction kinetics in such media. Previous research has concentrated on the influence of volume exclusion on equilibrium reaction constants[13,14] and on obtaining modified reaction rates based on the assumption of averaged isotropic (anomalous or normal) diffusion with reduced coefficients.[2,3] However, this classical approach ignores the strong modulation imposed on a binary reaction by the diffusive anisotropy that ensues from the local inhomogeneities of the obstacle configurations. Our analysis shows that this locally induced, long-lived anisotropy modulates strongly the overlap of the diffusing particles and hence skews the distribution of reaction rates toward low values. As time increases, the distribution of rates becomes centered around the averaged homogeneous prediction, but this only occurs on time scales longer than those observed or relevant in many applications. The implication is that averaging the local inhomogeneities of the nanoscale environment can lead to overestimation of the typical reaction rates of nanoparticulate systems in crowded media.

For the sake of concreteness, and because of its fundamental importance for a variety of biological functions such as signal transduction,[15] we have chosen to study intracellular diffusion. However, the main outcomes of our work are extensible to other similar nanoporous media. To perform our simulations, we construct a simple model that captures some essential features of the cellular environment. The interior of the cell is a prominent example of a nanoscale porous medium: the cytoplasm is densely filled with macromolecules,[14,16,17] mostly proteins, many of which are found to be immobile.[18] Between 10 and 40% of the total cell volume is occupied by macromolecules in concentrations comparable to those in protein crystals.[15]

* To whom correspondence should be addressed. E-mail: m.barahona@imperial.ac.uk.
† Institute for Mathematical Sciences.
‡ Present address: School of Biological Sciences, University of Edinburgh, United Kingdom.
§ Department of Chemistry.
∥ Department of Bioengineering.
¶ E-mail: Ramon.Grima@ed.ac.uk.
# E-mail: s.yaliraki@imperial.ac.uk.

10.1021/jp9025865
Published on Web 04/06/2010

Most of those molecules do not actively participate in a given reaction yet induce considerable obstruction, through volume exclusion or direct interactions, to the free diffusion of reacting molecules. This effect is commonly referred to as macromolecular crowding.[13]

The effects of crowding depend on the size of the tracer molecule, ranging from a 2-fold reduction in the diffusion coefficient of small molecules such as spin labels[19] to a 500- to 1000-fold reduction (compared to measurements in aqueous solutions) for large mobile particles of the size of vesicles,[17] the range of typical nanoparticles. Detailed data about the composition of the cytoplasm is not generally available with only rough average data known for simple organisms such as *E. coli*.[16] Moreover, pathways are in many cases located in distinct regions of the cell with specialized local environments. Given these constraints, we have developed a model that captures the general features recognized about crowding: (i) steric repulsion is of fundamental importance for macromolecular interactions and is always present;[13] (ii) homogeneous solutions of hard-sphere particles of radius ~3 nm occupying a fractional volume $\phi \sim 0.34-0.44$ are similar to the eukaryotic cytoplasm in their excluded volume effects on small mobile molecules;[20] (iii) a significant fraction of crowding obstacles may be immobile or confined to small regions (corralled) for long times due to binding with the cytoskeleton, membranes, or large macromolecular complexes (e.g., 50−70% of mRNA in the cytoplasm is immobile or corralled for tens of seconds[21]); (iv) the average hydrodynamic radius of an intracellular protein in the eukaryotic cytoplasm can be estimated to be 4 nm with a mass of 160 kDA.[22]

Methodology

Using the above information about the cellular environment as a basis for our simulations, we define a finite three-dimensional square box of side length 280 nm and fill it with randomly placed static spherical particles of radius 4 nm that can interpenetrate. These obstacles are distributed uniformly but are not allowed to fall inside a small spherical void of radius 4 nm in the center of the box. We have studied three number concentrations of obstacles: 8627, 17255, and 25725 particles, which correspond to fractional volumes $\phi = 1 - \exp(-nV_p) = 0.10$, 0.19, and 0.27, respectively. Here, n is the obstacle density and V_p is the volume of each obstacle[23] and, consequently, the fractional volume ϕ is an ensemble-averaged quantity. For each fractional volume, we generate $M = 100$ random uniform configurations of obstacles. Figure 1 shows a close-up of a particular obstacle configuration at $\phi = 0.27$, which is comparable to physiologically relevant conditions.[20] It has been shown[24] that for a spherical tracer of radius r moving in a sea of spherical immobile and interpenetrating obstacles of radius R, as in our simulations, there exists a percolating path through the medium provided the nondimensionalized number density $n^* = n(r + R)^3 < 0.84$. For the case $\phi = 0.27$, we have $n^* = 0.60$, thus implying that at this concentration a tracer particle will be able to diffuse through the medium, though significantly hindered by the obstacles. We emphasize that the static obstacles do not explicitly represent actual macromolecular structures but rather mimic the excluded volume effects produced by compartments, the cytoskeleton, and proteins immobilized by extensive binding to membranes. Once a random realization of the obstacle distribution has been generated, a single mobile tracer particle of radius 4 nm is placed in the spherical void in the center of the box at time $t = 0$ and Brownian motion is simulated via a Langevin equation. The diffusion coefficient is set equal to that given by the Einstein−Stokes law in water ($D_0 = 0.0535$ nm^2/ns), since the cytoplasmic viscosity is similar to that of water.[17,22] The time step for simulation is set to 1 ns which implies an average spatial displacement per time step of 0.327 nm, an order of magnitude smaller than the particle radius and much smaller than the observed displacements of the tracer particle. Simulations carried out with a time step of 0.25 ns showed no appreciable differences. The Brownian dynamics evolves under hard-sphere interactions of the mobile particle with the crowding agents: if the updated position is inside an obstacle, then the particle is not moved. We have imposed periodic boundary conditions, but finite-size effects have been checked for and avoided carefully by stopping the simulation when the particle travels a total distance of $L_{sim} = 65$ nm from the center of the box.

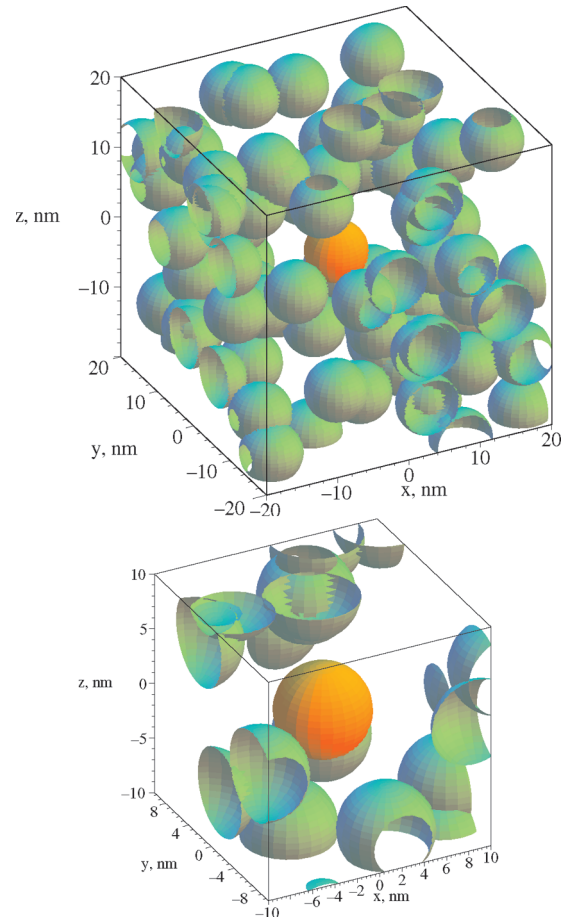

Figure 1. A typical realization of the obstacle distribution (green spheres) and the starting position of a mobile particle (orange sphere) at fractional volume $\phi = 0.27$, a density of obstacles similar to cellular crowding. Note that this is a close-up of a much larger box of size 280 nm in which the Brownian dynamics simulations are performed. The bottom figure is a zoom-in around the origin of the top figure, showing the ample space available for particle movement even at this obstacle density.

For each of the $M = 100$ realizations of the obstacle distribution, we repeat the Brownian dynamics simulation $N = 100$ times such that at each time point we have N different positions of the mobile particle providing a sample of the probability distribution of the diffusing particles, $P(\mathbf{r}, t)$. The deviation from sphericity of this distribution is a direct result of the spatial heterogeneity of the underlying obstacle distribution. The shape of $P(\mathbf{r}, t)$ can be characterized quantitatively using the time-varying gyration tensor (i.e., the inertia tensor with unit masses):[25]

$$T^m_{\alpha\beta}(t) = \frac{1}{2N^2}\sum_{i,j=1}^{N}(r^m_{\alpha,i}(t) - r^m_{\alpha,j}(t))(r^m_{\beta,i}(t) - r^m_{\beta,j}(t)) \quad (1)$$

where $r^m_{\alpha,i}(t)$ is the position of the ith particle at time t for the particular obstacle configuration $m = 1, \ldots, M$ and $\alpha = 1, 2, 3$ indicates the corresponding Cartesian component of the position vector. Hence, for each volume fraction, we obtain the time-dependent ellipsoidal characterization of the diffusive distribution from $M = 100$ distinct obstacle distributions. Instead of integrating the data from these random realizations into an isotropic, homogenized distribution, our approach will be to establish measures for both the anisotropy and shape of each ellipsoid which can then be averaged over the distribution.

Results and Discussion

Characterizing the Anisotropy of the Diffusive Distributions. In conventional simulation studies, one characterizes the diffusion in the crowded medium by performing an averaging of diffusive paths over all obstacle configurations to obtain a modified (reduced) mean square displacement (MSD) that is still isotropic. In contrast, our work focuses on the consequences of persistent, crowding-induced anisotropy—an effect that is washed out when such standard ensemble averaging is performed. However, we remark that our simulation data can also be used to computed ensemble-averaged isotropic measures and we have indeed checked that our results agree with those previously reported in the literature.[24] In particular, it has been shown[26] that a tracer particle in a sea of immobile obstacles will experience (isotropic) anomalous diffusion for short times and normal diffusion on longer time scales. We find the same in our simulations. Following Saxton (see Figure 1D in ref 26), one can compute the crossover time from anomalous to normal diffusion, T_c, by fitting two power law curves to the very short and very long time data on a graph of (MSD/t) versus t and calculating the time T_c at which these two lines intersect to obtain $T_c = 4500$ ns for $\phi = 0.1$, $T_c = 10000$ ns for $\phi = 0.19$, and $T = 116200$ ns for $\phi = 0.27$. The short-time data can then be used to characterize the anomalous diffusion regime. Denoting by α the short-time exponent for MSD, we find $\alpha = 0.91$ for $\phi = 0.1$, $\alpha = 0.84$ for $\phi = 0.19$, and $\alpha = 0.76$ for $\phi = 0.27$. Note that the short-time exponent for $\phi = 0.27$ agrees well with the experimental value of 0.73 ± 0.03 for a diffusing dextran molecule of radius 4.8 nm and mass 150 kDa inside a cell,[27] a fact that provides further justification for the number density and size of crowding agents used here as a rough model for the cytoplasm. It is important to remark that the total simulation times (23000 ns for $\phi = 0.1$, 50000 ns for $\phi = 0.19$, and 182000 ns for $\phi = 0.27$) are significantly longer than the crossover times for all fractional volumes. Hence, we can also characterize the normal diffusion regime at long times as indicated by the fact that, in all cases, the long-time exponents are close to unity. Our calculated long-term diffusion coefficients are consistent with those reported in the literature: $D/D_0 \simeq 0.6$ (**0.7**) for $\phi = 0.1$, $D/D_0 \simeq 0.3$ (**0.4**) for $\phi = 0.19$, and $D/D_0 \simeq 0.1$ (**0.1**) for $\phi = 0.27$, where D_0 is the aqueous diffusion coefficient in the absence of obstacles and the values in bold inside the parentheses are those roughly estimated from the paper by Hofling et al.[24]

In order to avoid the orientational averaging that washes away the intrinsic anisotropy of the local diffusion, we introduce a representation that retains a description of the overall shape of the spatial particle distribution, $P(\mathbf{r}, t)$. A natural first-order measure to describe the time evolution of the shape of the probability distribution for each obstacle distribution can be obtained from the eigenvalues $R_1 \leq R_3 \leq R_2$, and the associated eigenvectors, of the ellipsoids associated with the inertia tensor $T^m_{\alpha\beta}(t)$, given in eq 1. More specifically, the value of R_3 relative to the other two eigenvalues indicates whether $P(\mathbf{r}, t)$ can be best approximated by an egg/prolate ($R_3 \sim R_1$) or disk/oblate ($R_3 \sim R_2$) shape. Similarly, the deviation of $P(\mathbf{r}, t)$ from sphericity (i.e., the anisotropy) is measured by the condition number (or maximum aspect ratio) $\Lambda = (R_2/R_1)^{1/2}$, where $\Lambda = 1$ for the sphere. Using these definitions, we calculate the shapes and anisotropy of the ellipsoids obtained from $P(\mathbf{r}, t)$ at all times for each of the 100 distinct realizations of the obstacles. Figure 2 illustrates how the ellipsoids computed from our simulation data enable us to study the change in time of the shape of the distributions of mobile particles. As expected, the distribution of walkers for a given obstacle distribution shows decreasing anisotropy as time evolves. At very long times, the corresponding ellipsoids become nearly spherical.

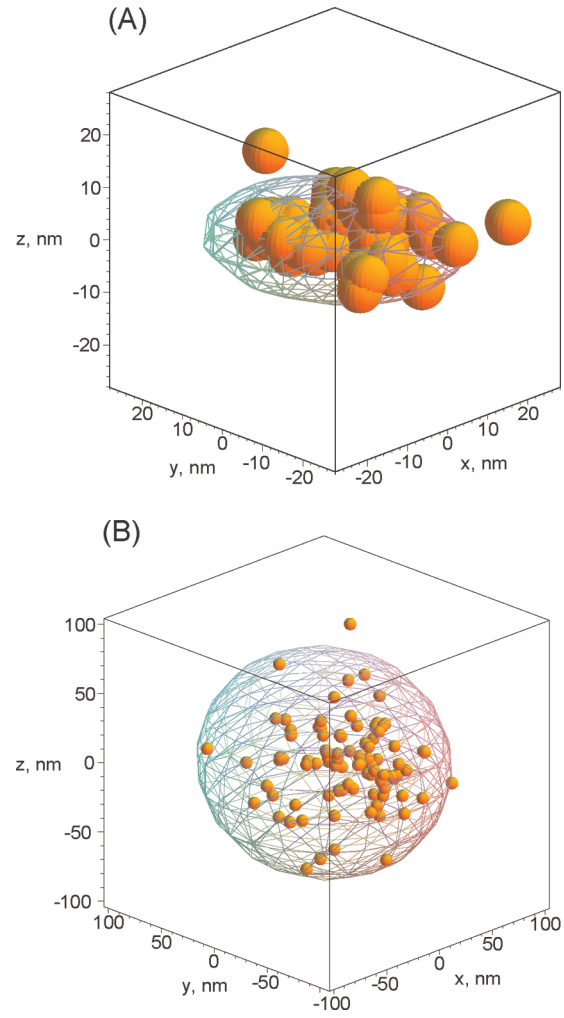

Figure 2. Quantification of the spatial anisotropy of the probability distribution of mobile particles with the gyration tensor. The figure represents the positions of 100 mobile particles (orange spheres) diffusing with Brownian dynamics in one realization of the obstacle distribution with volume fraction $\phi = 0.27$. The gyration tensor defined in eq 1 captures the shape of the distribution of the mobile particles at (A) short times (1.2 μs) and (B) long times (102.8 μs). The obstacles have not been drawn for clarity.

Our results show that the crowding-induced anisotropy is long-lived when the excluded volume is high. Figure 3 presents the time evolution of the maximum aspect ratio of the ellipsoids

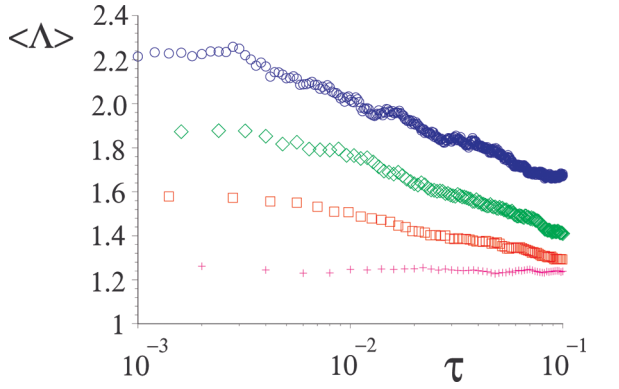

Figure 3. Maximum aspect ratio of the ellipsoids averaged over all obstacle configurations $\langle\Lambda\rangle$ for different volume fractions as a function of the adimensional time $\tau = t(D/L_{sim}^2)$, where $L_{sim} = 65$ nm is the length scale spanned by our simulations and $D(\phi)$ is the diffusion coefficient, which depends on the obstacle density. This normalized time allows us to represent the diffusive dynamics at different obstacle densities (see text). The ellipsoids approximate the shape of the probability distribution of a 4 nm mobile protein or nanoparticle diffusing in a heterogeneous random distribution of spherical, static particles with volume fraction ϕ. The data is for $\phi = 0$ (crosses, magenta), $\phi = 0.10$ (squares, red), $\phi = 0.19$ (diamonds, green), and $\phi = 0.27$ (circles, blue). The average $\langle\Lambda\rangle$ is found to coincide with the mode of the distribution of Λ at any given time (data not shown), implying that it is representative of the diffusion anisotropy.

averaged over obstacle distributions, $\langle\Lambda\rangle$, for fractional volumes $\phi = 0.1, 0.19$, and 0.27 and for control simulations with no obstacles ($\phi = 0$) under the same number of realizations: 100 distinct sets of 100 random walkers. In the figure, we nondimensionalize time via the scaling $\tau = t(D/L_{sim}^2)$, where $L_{sim} = 65$ nm is the length scale spanned by our simulations. This scaling provides a normalization of the simulation (real) time with respect to the time it takes for a particle to diffuse a given distance at different obstacle densities. As expected, the distribution of diffusing particles is always close to sphericity for $\phi = 0$: the maximum aspect ratio is constant in time and close to 1, $\langle\Lambda\rangle_{iso} \sim 1.24$. The observed deviation from unity is due to the small sample size ($N = 100$), as confirmed by additional simulations (not shown) for larger numbers of particles, $\langle\Lambda\rangle_{iso} \sim 1.07$ for $N = 1000$, and it approaches 1.0 in the limit of large N.

In contrast, the distributions are significantly anisotropic in the presence of obstacles. For short times, the anisotropy is roughly proportional to the fractional excluded volume: $\langle\Lambda\rangle - \langle\Lambda\rangle_{iso} \propto \phi$. This is a reflection of the fact that local voids become more anisotropic as the obstacle concentration increases toward the percolation limit. As time grows, the anisotropy decreases. At the physiologically relevant volume fraction ($\phi = 0.27$), the asymmetry is high (maximum aspect ratio greater than 2) for times of the order of a few microseconds and approaches isotropy following a power law behavior of the form $t^{-0.27}$ in the time range 3−182 μs. We have checked that this behavior is not dependent on the particular measure of anisotropy chosen: the asphericity Δ,[28,29] an alternative measure, yields an exponent equal to −0.26. An extended power law appears to exist only for volume fractions close to the percolation threshold. (The decay is more complex for $\phi = 0.1$ and 0.19, and we have not attempted to extract an exponent in these cases.) The slow decay of the anisotropy means that at the maximum simulation time of 182 μs, the distribution at $\phi = 0.27$ is still significantly asymmetrical, with $\langle\Lambda\rangle \simeq 1.6$, even though the particle has on average traveled a distance of 65 nm, a length scale comparable to that of some organelles. This suggests that anisotropic diffusion can persist across large regions of the cell and that it can arise from mechanisms unrelated to active directed transport along microtubules.

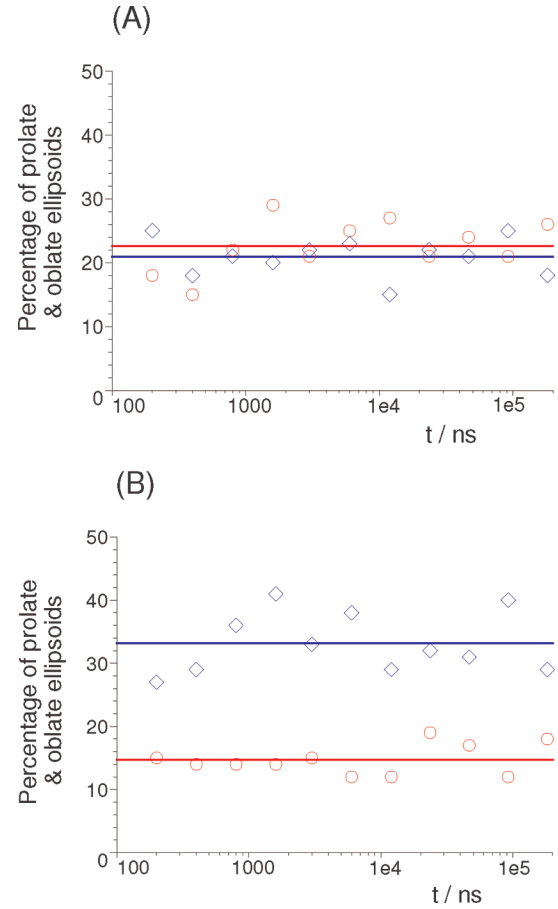

Figure 4. Percentage of prolate (blue diamonds) and oblate ellipsoids (red circles) averaged over 100 distinct obstacle realizations as a function of time for (A) $\phi = 0$ and (B) $\phi = 0.27$. The solid lines show the time-averaged percentages.

Characterizing the Shape of the Diffusive Distributions. Our simulations can also be used to quantify the overall geometrical shape of the probability distribution as a function of time and crowding density. The shape of the ellipsoid that approximates the distribution is determined by the aspect ratios $\Lambda = (R_2/R_1)^{1/2}$ and $\lambda = (R_3/R_1)^{1/2}$. Note that $1 \le \lambda \le \Lambda$. If λ is closer to 1 than to Λ, the ellipsoid is prolate; if λ is closer to Λ than to 1, the ellipsoid is oblate. This idea can be captured quantitatively by splitting the range of λ into three equal regions: (i) if $1 \le \lambda \le 1 + {}^1/_3(\Lambda - 1)$, the ellipsoid is prolate; (ii) if $1 + {}^2/_3(\Lambda - 1) \le \lambda \le \Lambda$, the ellipsoid is oblate; (iii) otherwise, it is classified as neither. Using this measure, we calculate in Figure 4 the percentage of prolate and oblate ellipsoidal distributions as a function of time. As expected, in the absence of crowding, the percentage of prolates (20.9%) is approximately equal to that of oblates (22.6%). However, crowding breaks this symmetry, leading to 2.3 times more prolates (33.2%) than oblates (14.7%) when $\phi = 0.27$. These percentages appear to be relatively time-independent. Note that this observation is not at odds with the results in Figure 3: the distribution of diffusing particles can approach isotropy yet keeping its predominantly prolate character. Again, these findings do not depend on the particular measure of shape used: the ratio of prolate to oblate ellipsoids, measured according to the shape factor S,[29] also jumps from 1.1 at $\phi = 0.1$ to 2.9 at $\phi = 0.27$. The preponderance of prolate shapes induced by crowding is the result of diffusion

proceeding in each local environment along one preferred direction: Ideal prolate distributions are formed if the obstacle distribution is characterized by one direction along which the number of obstacles is small compared to that along all other directions. On the other hand, oblate distributions require that the number of obstacles is comparatively small along directions on a plane. Hence, high crowding favors prolate distributions.

Characterizing the Effect on Reaction Kinetics. Beyond implications for pure transport, this persistent anisotropic transport with prolate dominance has a crucial effect on chemical reaction rates in crowded environments. To quantify its influence, we use the following simple scenario. Consider two types of molecules that react upon encounter with some probability and which are produced continuously at two different spatial sites in the cytoplasm. The reaction rate at a given time is proportional to the probability of encounter of a pair of different molecules at any point in space at that time. If the particles are diffusing, this is given by the integral over all space of the joint probability distribution of the positions of mobile particles at time t, otherwise known as the overlap integral $I(t)$. Our gyration tensor gives an ellipsoid centered on a spatial site, which approximates the shape of the corresponding probability distribution. This leads to an anisotropic Gaussian probability density function whose main axes point in the direction of the eigenvectors of the tensor T and the variances in each direction equal the radii squared, i.e., the eigenvalues of T. It can be shown[30] that the overlap integral $I(t)$ of the diffusing particles from both centers is given by

$$I(t) = \frac{C}{\sqrt{\mathrm{Det}(\mathbf{A}+\mathbf{B})}} \exp\left[-\frac{1}{2}\mathbf{R}^T(\mathbf{A}^{-1}+\mathbf{B}^{-1})^{-1}\mathbf{R}\right] \tag{2}$$

Here, $\mathbf{A}(t) = \sum_{i=1}^{3} a_i^{-2}\mathbf{u}_i \otimes \mathbf{u}_i$ and $\mathbf{B}(t) = \sum_{i=1}^{3} b_i^{-2}\mathbf{v}_i \otimes \mathbf{v}_i$, where a_i (respectively, b_i) are the time-varying semiaxes along the corresponding time-dependent normalized eigenvectors $\mathbf{u}_i$ (respectively, $\mathbf{v}_i$) of the diffusional ellipsoids centered at site $\mathbf{R_A}$ (respectively, $\mathbf{R_B}$). The normalization constant C is equal to $((8\pi^3)^{1/2}\prod_{i=1}^{3} a_i b_i)^{-1}$, and $\mathbf{R} = \mathbf{R_B} - \mathbf{R_A}$ is the distance vector between the two diffusive centers. Note that, for two isotropic Gaussian density functions, eq 2 reduces to the well-known result: $I_{\mathrm{iso}}(t) = \exp(-||\mathbf{R}||^2/4\sigma^2)/(8\pi^{3/2}\sigma^3)$, where $\sigma^2(t)$ is the time-dependent variance of both Gaussians.

The overlap integral $I(t)$ exerts a modulation on the reaction rate of the reaction due to the diffusive behavior. In order to quantify the effect of crowding on reaction kinetics, we use our simulations as follows. The diffusion originating in a particular local environment is described by the time-varying ellipsoid of mobile particles for a particular obstacle realization. Hence, we can use the $M = 100$ obstacle configurations generated for each volume fraction to study the time-dependent overlap integral $I(t)$ for the $\binom{100}{2}$ distinct pairs of configurations. This method effectively simulates the reaction kinetics of around 5000 independent systems with molecule production at two spatial sites independently drawn from the same random distribution of obstacle configurations with fraction volume ϕ. The sites could either represent different cells or different regions of a single cell. We expect this procedure to approximate well the scenario of two-site molecule production for short to intermediate times, when the average width of the distribution $P(\mathbf{r}, t)$ is smaller than $||\mathbf{R}||/2$, i.e., precisely the regime when the anisotropic effects are most significant.

Using the above procedure, we can obtain the distribution of reaction rates at each value of ϕ. We show in Figure 5 the density and the cumulative distribution functions of $I(t)$ for $\phi = 0.27$ at two specific times for two sites situated at a distance of $||\mathbf{R}|| = 30$ nm. For short times ($t = 4$ μs), the distribution of rates is monotonically decreasing and hence it is not humped around the mean; i.e., the typical values of the reaction rates are smaller than the average. As time grows, the distribution becomes unimodal and centered around the mean, so that the average rate represents the typical behavior, as seen for $t = 12$ μs. In terms of the cumulative distribution, this means that, for $\phi = 0.27$, almost 80% of the values of $I(t = 4\ \mu\mathrm{s})$ are less than the average, whereas, for $t = 12$ μs, this proportion reduces to 57%. This result also implies that only as time becomes large does the average value of the distribution match the expected value of $I(t)$ for a homogenized medium with the same volume fraction. We have checked this explicitly by performing computations averaged over all obstacle configurations, which lead to isotropic distributions, and obtaining the value of the overlap integral in this case (Figure 5).

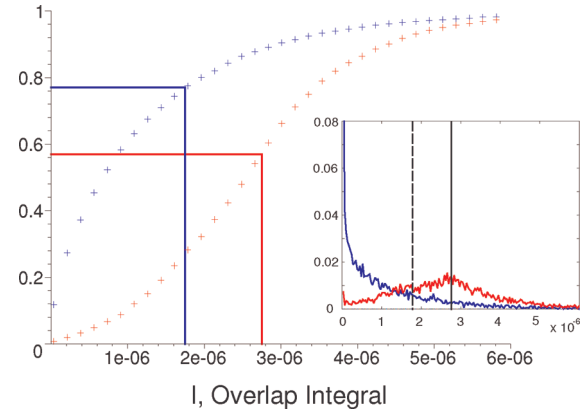

Figure 5. Cumulative distribution of the overlap integral $I(t)$ in eq 2 for ~5000 independent systems of reactants diffusing from two spatial sites separated by a distance of $||\mathbf{R}|| = 30$ nm. The spatial sites are different realizations of the obstacle distribution at $\phi = 0.27$. The overlap integral is a diffusive prefactor that modulates the kinetic rate of the reaction. We show distributions of $I(t)$ representative of short times ($t = 4$ μs, blue curve), when the anisotropy is most significant, and longer times ($t = 12$ μs, red curve), when the anisotropic effects are less dominant. The solid vertical lines indicate the unique value of $I(t)$ obtained for a perfectly homogenized obstacle distribution at the same volume fraction $\phi = 0.27$. For $t = 4$ μs, the homogenized value of $I(t)$ is larger than 77% of the heterogeneous rates, whereas this percentage is reduced to 57% for $t = 12$ μs. The probability distribution of $I(t)$ (inset) indicates that the distribution at short times is monotonically decreasing, hence biased toward values lower than the homogenized expectation. As time grows, the distribution becomes unimodal and the typical behavior approaches the expected homogeneous rate, indicated by the vertical lines (dashed for $t = 4$ μs and solid for $t = 12$ μs).

These results indicate that the anisotropic transport induced by local inhomogeneities has a direct effect on the kinetics (or collision events), since the overlap of two diffusive distributions is highly dependent on their shapes and orientations. Therefore, the kinetic rates are significantly different in a heterogeneous medium and a homogenized medium even if they have nominally the same crowding. This can be understood as follows. The pre-exponential factor in eq 2 is approximately equal to the inverse of the average volume of the two ellipsoids. As follows from our previous discussion, the volume of the ellipsoids is similar to the corresponding spherical volume of the homogenized case at all times—a reflection of the similarity of both media in an average sense. For instance, our numerical simulations show that the average volume of the ellipsoids is 532 ± 305 nm^3 at $t = 4$ μs and 1857 ± 1024 nm^3 at $t = 12$ μs,

whereas the spheres calculated from the homogenized case have volumes of 661 and 2177 nm^3, respectively. Hence, the pre-exponential factor of the anisotropic and homogenized cases is similar at all times. As time grows, the volume of the ellipsoids grows and the pre-exponential factor dominates, leading to similar rates for the heterogeneous and homogenized cases for long times. On the other hand, for short times, the ellipsoids have small volumes and are far from each other; hence, the overlap integral is dominated by the argument of the exponential. The argument of the exponential in $I(t)$ can be related, through an inverse dependence, to the directional distance of closest approach between the ellipsoids, a distance that is strongly dependent on the anisotropy.[30,31] In particular, the directional distance of closest approach between two nonoverlapping prolate ellipsoids is generally larger than the surface-to-surface distance between two spheres of the same volume placed at the same intercenter distance. This induces a dramatic reduction of the overlap integral for prolates as compared to the spherical case. Because of the preponderance of prolates, the heterogeneous reaction rates will be thus biased toward smaller values than the homogenized expectation at short and intermediate times.

Conclusion

Our results suggest that calculations and simulations of reaction kinetics in crowded environments under the assumption of homogeneous spatial density can severely overestimate the rates of reactions. Although it is generally accepted that *diffusion-limited* reactions would proceed slower due to the diminished magnitude of the average (homogenized and isotropic) transport coefficients, our study suggests that this slowdown is significantly aggravated by diffusion anisotropy due to the medium's inherent nanoscale structural architecture. In particular, the averages are not typical of those seen in an ensemble of heterogeneous distributions at the same excluded volume fraction. Our proposed method quantifies the anisotropic transport properties of (mesoscopically homogeneous) random porous media and shows how the deviations from isotropy play a major role in determining the distributions of reaction rates and consequently the time course of reactions inside these media. This inherent anisotropic diffusion transport of reactants is implicitly ignored when invoking the standard orientational averaging. Clearly, these anisotropic effects would not play a major role in the dynamics of reaction-limited reactions, since diffusion is not the limiting factor in such cases.

In this respect, it is also worth mentioning that, although our results indicate a reduction of molecular association rates due to crowding, it is also possible that crowding can enhance macromolecular association rates. This effect depends on the magnitude of the crowding. As first discussed by Minton in terms of scaled particle theory[32] and recently shown using simulations,[33] enhancement of association rates can be obtained for small crowding while the opposite is observed for large crowding. Essentially, any diffusion-limited reaction will occur at a lower rate in the presence of crowding, since diffusion transport is decreased by the obstacles.

In this work, we have concentrated on the case where obstacles are assumed to be immobile. Although in general intracellular obstacles can be mobile or immobile on time scales relevant to reactions between tracer particles, it is important to remark that the anisotropy of a tracer particle in a mixture of mobile and immobile particles is dictated by the immobile fraction, since the latter form the labyrinth through which both tracer and mobile particles will move. For example, if a tracer particle finds itself in a local cage of immobile obstacles in which there is just one exit direction, the addition of mobile obstacles in the cage will naturally make it more difficult for the tracer to diffuse out of the cage, but the anisotropy of the movement is still preserved because the exit direction is dictated exclusively by the local immobile obstacle distribution. The mobile fraction simply hinders the movement of the tracer through this fixed labyrinth of immobile obstacles and hence only affects the magnitude of the long-time isotropic diffusion coefficients but has no impact on the anisotropy measures reported herein.

We expect these anisotropic effects to influence the transport of nanoparticles in crowded environments encountered in nanobiological applications. Indeed, these effects will become even more significant when the obstacles themselves are anisotropic, as is the case in realistic systems. This will be an area of future research. Particle tracking in experimental techniques such as single[34] and multiple particle tracking[35] may also be used to measure these effects at appropriate volume fractions. Although we have described our findings in the context of a model for the intracellular environment, these results are broadly applicable to general nanoscale porous media.

References and Notes

(1) Torquato, S. *Random Heterogeneous Materials*; Springer-Verlag: New York, 2002.
(2) Kopelman, R. *Science* **1988**, *241*, 1620.
(3) Grima, R.; Schnell, S. *Biophys. Chem.* **2006**, *124*, 1.
(4) Zürner, A.; et al. *Nature* **2007**, *450*, 705.
(5) Kirstein, J.; et al. *Nat. Mater.* **2007**, *6*, 203.
(6) Roy, I.; et al. *Proc. Natl. Acad. Sci. U.S.A.* **2005**, 102–279.
(7) Chavanpatil, M. D.; Khdrai, A.; Panyam, J. *Pharm. Res.* **2007**, *24*, 803.
(8) Morgan, T. T.; et al. *Nano Lett.* **2008**, *8*, 4108.
(9) Kester, M.; et al. *Nano Lett.* **2008**, *8*, 4116.
(10) Popovtzer, R.; et al. *Nano Lett.* **2008**, *8*, 4593.
(11) Heller, D. A.; et al. *Science* **2006**, *311*, 508.
(12) Kim, S. A.; Heinze, K. G.; Schwille, P. *Nat. Methods* **2007**, *4*, 963.
(13) Minton, A. P. *J. Biol. Chem.* **2001**, *276*, 10577.
(14) Schnell, S.; Turner, T. E. *Prog. Biophys. Mol. Biol.* **2004**, *85*, 235.
(15) Bray, D. *Annu. Rev. Biophys. Biomol. Struct.* **1998**, *27*, 59.
(16) Goodsell, D. S. *Trends Biochem. Sci.* **1991**, *16*, 203.
(17) Luby-Phelps, K. *Int. Rev. Cytol.* **2000**, *192*, 189.
(18) Clegg, J. S. *Am. J. Physiol. Regulatory Integrative Comp. Physiol.* **1984**, *246*, 133. Fulton, A. B. *Cell* **1982**, *30*, 345.
(19) Mastro, A. M.; et al. *Proc. Natl. Acad. Sci. U.S.A.* **1984**, *81*, 3414.
(20) Zimmerman, S. B.; Trach, S. O. *J. Mol. Biol.* **1991**, *222*, 599.
(21) Fusco, D.; et al. *Curr. Biol.* **2003**, *13*, 161.
(22) Bicout, D. J.; Field, M. J. *J. Phys. Chem.* **1996**, *100*, 2489.
(23) Garboczi, E. J.; et al. *Phys. Rev. E* **1995**, *52*, 819.
(24) Hofling, F.; Franosch, T.; Frey, E. *Phys. Rev. Lett.* **2006**, *96*, 165901.
(25) Bishop, M.; Michels, J. P. J. *Chem. Phys. Lett.* **1985**, *82*, 1059.
(26) Saxton, M. J. *Biophys. J.* **1994**, *66*, 394.
(27) Weiss, M.; et al. *Biophys. J.* **2004**, *87*, 3518.
(28) Rudnick, J.; Gaspari, G. *J. Phys. A: Math. Gen.* **1986**, *19*, 191.
(29) Dima, R. I.; Thirumalai, D. *J. Phys. Chem. B* **2004**, *108*, 6564.
(30) Perram, J. W.; et al. *Phys. Rev. E* **1996**, *54*, 6565.
(31) Paramonov, L.; Yaliraki, S. N. *J. Chem. Phys.* **2005**, *123*, 194111.
(32) Zimmerman, S. B.; Minton, A. P. *Annu. Rev. Biophys. Biomol. Struct.* **1993**, *22*, 27.
(33) Kim, J. S.; Yethiraj, A. *Biophys. J.* **2009**, *96*, 1333.
(34) Jin, H.; Heller, D. A.; Strano, M. S. *Nano Lett.* **2008**, *8*, 1577.
(35) del Alamo, J. C.; et al. *Proc. Natl. Acad. Sci. U.S.A.* **2008**, *105*, 15411.

JP9025865